Non-linear viscoelasticity of hagfish slime

Randy H. Ewoldt [a],*, Timothy M. Winegard [b], Douglas S. Fudge [b]

[a] Institute for Mathematics and its Applications & Department of Chemical Engineering and Materials Science, University of Minnesota, Minneapolis, MN 55455, USA
[b] Department of Integrative Biology, University of Guelph, Guelph, ON, Canada N1G 2W1

ABSTRACT

We report here the first experimental measurements of non-linear rheological material properties of hagfish slime, a hydrated biopolymer/biofiber network, and develop a microstructural constitutive model to explain the observed non-linear viscoelastic behavior. The linear elastic modulus of the network is observed to be $G' \approx 0.02$ Pa for timescales $0.1 \text{ s} \leq t \leq 10 \text{ s}$, making it one of the softest elastic biomaterials known. Non-linear rheology is examined via simple shear deformation, and we observe a secant elastic modulus which strain-softens at large input strain while the local tangent elastic modulus strain-stiffens simultaneously. This juxtaposition of simultaneous softening and stiffening suggests a general network structure composed of non-linear elastic strain-stiffening elements, here modeled as finite extensible non-linear elastic (FENE) springs, in which network connections are destroyed as elements are stretched. We simulate the network model in oscillatory shear and creep, including instrument effects from rotational inertia. The network model captures the simultaneous softening of the secant modulus and stiffening of tangent modulus as the model enters the non-linear viscoelastic regime.

© 2010 Elsevier Ltd. All rights reserved.

1. Introduction

Hagfishes are marine animals that inhabit the cool or deep parts of the oceans of both hemispheres [1]. They have long bodies (Fig. 1a), and are sometimes called "slime eels" although they are not eels at all. Hagfishes are well known for their ability to produce large amounts of slime when they are provoked or stressed. They do this by ejecting a small amount of *exudate* (Fig. 1b) which can mix into a large volume of the surrounding water, forming a mucus-like cohesive mass [2–4]. The resulting material is hypothesized to serve as a defense mechanism against predators [5]. Here we are interested in the leading order non-linear mechanical properties of such a resulting cohesive mass of hagfish slime.

Hagfish slime is distinct from other mucus-like materials. In addition to mucin-like molecules it also contains a fibrous component made of protein-based intermediate filaments [6,7]. The diameter of these intermediate filament threads ranges from 1 to 3 μm, and when fully unraveled the length can be about 15 cm long [8]. The unraveling of thread skeins is important for setting up the gel-like network structure. It has recently been shown that at least some of the *mucin* components are able to elongate into strands that appear to be important for unraveling of the long thread skeins [9]. The resulting hagfish slime network is therefore a hierarchical material structure. At t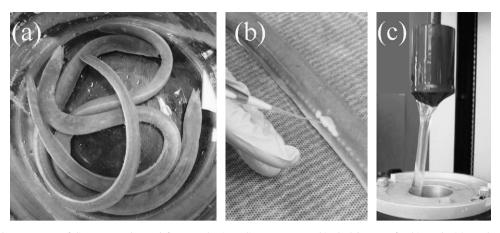he largest lengthscale it is a sticky network of extended threads and mucin-like biopolymers. The threads themselves are composed of tightly packed and aligned intermediate filaments (IFs) [10], and each IF is composed of keratin-like proteins [6,7] which have been shown to undergo an irreversible conformational change from $\alpha-$helix to $\beta-$sheet under large deformation [10].

One remarkable thing about hagfish slime is that small volumes of exudate can entrain large volumes of water. A typical slime mass created by a hagfish has a volume of about 0.9 l, but is created from only 90 mg of exudate (0.1 mg/ml) [8]. The exudate is about 66% water, so the dry weight fraction is smaller yet, containing only about 20 mg of slime threads and 15 mg of mucins (0.04 mg/ml dry weight) [8]. In contrast, typical human mucin concentrations are about $1000 \times$ larger (47 mg/ml for gastric, 37 mg/ml for duodenal, and 20 mg/ml for colonic mucus) [11]. The slime mass network of exudate mixed with seawater is an ultra-dilute material structure, which can accommodate large stretch ratios while entraining seawater. For sufficiently short times there is minimal draining of water, and the slime can be lifted into the air while the network remains a cohesive mass (Fig. 1c). The viscous entrainment of large volumes of water enables the most likely function of hagfish slime, which is to thwart attacks by gill-breathing predators [5].

The functional properties of hagfish slime depend on the mechanical properties of the resulting network. Furthermore, the peculiar nature of hagfish slime inspires the possibility of a bio-inspired ultra-dilute elastic network which can be similarly deployed as a defensive or clogging mechanism for engineered systems. However, until now only a limited number of studies have characterized the mechanical

* Corresponding author.
    E-mail address: ewoldt@ima.umn.edu (R.H. Ewoldt).

Fig. 1. Hagfish produce large amounts of slime as a predatory defense mechanism. Slime was prepared in the laboratory for this study; (a) top-down view of three Atlantic hagfish in a large glass beaker; (b) exudate is collected from an anesthetized hagfish with a pipette and then mixed with seawater to form "hagfish slime," an ultra-dilute network of polymeric mucus and fibrous protein threads, shown in (c) with the rotational rheometer geometry in the raised position after testing, demonstrating that hagfish slime networks can sustain large stretch ratios while maintaining a cohesive mass that adheres to the test geometry.

properties of hagfish slime and its components. Tensile measurements of individual threads indicate that the hydrated intermediate filaments have an initial tensile modulus of approximately $E = 6.4$ MPa [10]. The full hagfish slime network includes threads and mucin-like molecules, and experimental mechanical measurements of whole slime networks have also been performed by Fudge et al. [8]. The difficulty of mixing and testing hagfish slime led them to use a plunger/beaker apparatus with spikes at the bounding surfaces. The setup was successful, but imposed a complicated deformation field and could not measure intrinsic material properties of the network such as viscoelastic moduli. Recently, Fudge et al. successfully used a commercial rheometer to measure viscoelastic properties of hagfish slime [12], where an elastic modulus of a hagfish network was first reported to be $G \approx 0.02$ Pa. This is about five orders of magnitude more compliant than materials like gelatin, making it one of the softest elastic biomaterials known.

The primary obstacles of testing a slime network on a rheometer are sample mixing, sample contact with the bounding surface, and measurements of the ultra-soft network which can suffer from instrument artifacts. In this work we extend the sample preparation technique used in [12] for testing hagfish slime on a rheometer, while paying careful attention to the artifacts introduced when testing such a soft sample. We report for the first time both time-dependent and amplitude-dependent material properties of hagfish slime in simple shear deformation. We report frequency-dependent linear viscoelastic moduli over two decades of frequency, 0.1 rad s$^{-1} < \omega < 10$ rad s^{-1}. The non-linear mechanical properties are examined with large amplitude oscillatory shear (LAOS) tests which impose increasing strain amplitude γ_0 at fixed frequency ω. The non-linear mechanics are further examined with creep compliance tests over a range of stress amplitudes σ_0.

In addition to the new experimental results, we develop a non-linear network model constitutive theory to describe the prominent features of the response. The microstructural theory is based on the idea of a network structure composed of non-linear elastic strain-stiffening elements, here modeled as finite extensible non-linear elastic (FENE) springs, in which network connections are destroyed as elements are stretched. We simulate the model response to experimental conditions, including the effects of instrument inertia. The inertio-elastic oscillations are deliberately utilized to examine the non-linear viscoelastic properties and to compare the experimental measurements with the structure–property relationships of the model.
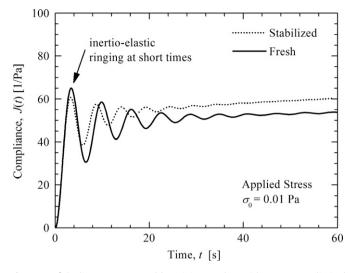
2. Material and methods

2.1. Rheometry methods

Viscoelastic properties of the slime were measured with a torque-controlled rheometer (AR-G2, TA Instruments) using a concentric-cylinder geometry (a.k.a. cup-and-bob). Tests were temperature controlled by a Peltier system to maintain $T = 10\ ^\circ$C, rather than room temperature, to more closely match the cool temperatures of natural hagfish habitats. The geometry consists of an outer cup with flat bottom (radius $R_o = 15$ mm). The inner cylinder has radius $R_i = 14$ mm, length $L = 41.5$ mm over which the radius is constant, and a protruding conical bottom with half angle $\theta/2 = 60^\circ$.

The mixed sample of slime was placed in the cup, and the inner cylinder lowered into the sample until the bottom conical point reached a distance $h = 5$ mm from the bottom of the cup, pushing the sample into the 1 mm gap between the inner and outer cylinders. The total sample volume $V = 12$ ml was chosen such that the sample exactly reached the top of the inner cylinder. The sample is thus contained around and below the inner cylinder. It is the portion of the sample confined in the small gap which dominates the resistance to deformation, and this deformation is approximately described as simple shear, with strain-rate $\dot{\gamma} \simeq \Omega R_i / (R_o - R_i)$, where Ω is the angular velocity, R_i is the inner radius, and R_o is the outer cylinder radius.

The rheological tests performed here involve simple shear deformation, with both displacement-control and torque-control tests. Oscillatory shear tests are executed under controlled deformation conditions, i.e. the strain-rate is specified as $\dot{\gamma}(t) = \dot{\gamma}_0 \cos(\omega t)$, and the viscoelastic stress response is examined as a function of frequency ω and amplitude γ_0. Shear flow tests were attempted, but were unsuccessful due to the wrapping of the slime threads around the inner rotor of a cup-and-bob geometry. A cone-plate geometry was also used, but in this case the solid mucus/thread components wrapped around themselves and aggregated in the center of a saltwater puddle. The experimental results presented here involve small to moderate shear deformations, but even at these modest deformations a non-linear mechanical response is clearly evident.

Creep tests are also performed, in which the applied torque load is a step function and the resulting displacement is measured. The material sample is so soft, $G' \approx 0.02$ Pa (Fig. 2), that under these stress-input conditions the rotational inertia of the instrument can

Fig. 2. Hagfish slime was prepared by mixing exudate with seawater. A limited amount of "fresh" exudate was available to be mixed immediately with seawater and tested, whereas additional exudate samples were "stabilized" in mineral oil for shipment and mixed with seawater remotely. Data for the fresh sample was originally reported in [12]. The rheological response is remarkably comparable for the fresh and stabilized samples. At short times inertio-elastic ringing is observed, in which the sample elasticity couples with the finite instrument rotational inertia to "ring" at a resonant frequency, just like a mass at the end of a spring (see Section 4.2). The initial secant moduli are $G_0 = 0.0207$ Pa (stabilized) and $G_0 = 0.0218$ Pa (fresh). The stabilized sample exhibits a higher frequency of intertio-elastic oscillations, indicating a larger tangent modulus $K' = 0.0435$ Pa, compared to $K' = 0.0291$ Pa for the fresh sample.

significantly alter the displacement response to imposed torque loading. The rotational geometry takes time to accelerate and may furthermore oscillate via "inertio-elastic" oscillations, in which the sample elasticity couples with the finite instrument rotational inertia to "ring" at a resonant frequency, just like a mass at the end of a spring [13–15]. A careful analysis of the inertio-elastic oscillations can reveal both linear and non-linear viscoelastic properties of the sample [15]. The low modulus of hagfish slime adds difficulty to the experimental characterization due to the resulting dominant role of instrument inertia, but we will make use of the analysis of inertio-elastic oscillations to extract meaningful non-linear rheological properties. The detailed calculations associated with the inertio-elastic ringing analysis are outlined in Section 4.2.

2.2. Hagfish slime preparation

Specimens of Atlantic hagfish (*Myxine glutinosa*) were collected at the Huntsman Marine Science Centre and maintained at the University of Guelph as described by Winegard et al. [9]. Exudate was obtained from anesthetized hagfish as described in [9]. Hagfish were removed from a salt water containment bath, placed on a cold tray, and patted dry with a towel. Hagfish were then induced to produce slime exudate by electrical stimulation. Exudate was collected directly from the skin of the animal. Fig. 1b shows the collection of exudate using a pipette; glands line the body of the animal and appear in the image as light colored spots, whereas the exudate is the bigger white spot near the end of the pipette. For some tests, hagfish were available at the site of mechanical testing and "fresh" exudate could be used immediately for rheometry tests. Other tests were performed on exudate collected at the University of Guelph, in which case "stabilized" exudate was maintained under mineral oil and stored on ice for transport to the testing location [16].

To prepare the biopolymer network, a precise volume of exudate ($V_e = 10$ μl) was acquired using a micropipette, and this exudate was added to a predetermined volume of salt water ($V_{sw} = 12$ ml) in a Falcon tube. The tube was closed and the contents mixed to establish the slime gel network. Mixing was generated by sloshing the contents back and forth along the container axis by repeatedly inverting the tube. After mixing for six oscillations, the entire volume of sample material appeared fibrous and behaved as a cohesive mass. The resulting concentration of exudate is approximately 0.83 mg/ml (exudate mass to total network volume), assuming that the density of the exudate is close to $\rho = 1$ g/ml. This is a reasonable estimate since approximately 66% of the exudate mass is water [8]. The concentration of exudate was chosen to consistently entrain the full volume of salt water into the slime network, but we note that 0.83 mg/ml is more concentrated than naturally produced hagfish slime (0.1 mg/ml slime exudate to network volume [8]), presumably because hagfish utilize better mixing conditions to setup the network in vivo.

We compare "stabilized" and "fresh" exudate in Fig. 2 by showing the results from a single creep test on each sample type. For the creep tests a small constant load was imposed (shear stress $\sigma_0 = 0.01$ Pa) and the resulting strain $\gamma(t)$ observed as a function of time. Fig. 2 shows the creep compliance, defined as $J(t) = \gamma(t)/\sigma_0$. The data for the fresh sample was previously reported [12]. The stabilized exudate reported here shows remarkably comparable properties to the fresh exudate, despite the potential for aging, destabilization, or mixing conditions to modify the material properties. We therefore have confidence that rheological measurements using stabilized slime represent the fundamental character of fresh hagfish slime networks.

The inertio-elastic ringing response of Fig. 2 was analyzed following the procedures outlined in Section 4.2. The "ringing" modulus is interpreted here as the local tangent modulus about an imposed stress (i.e. the tangent modulus at $\sigma_0 = 0.01$ Pa) [15]. For a *non-linear* elastic response, the tangent elastic modulus $K' = d\sigma/d\gamma$ is different than the secant modulus $G = \sigma_0/\gamma$. The inertio-elastic oscillations allow for computation of both the tangent modulus K' and secant modulus G_0. The initial secant moduli for the samples are $G_0 = 0.0207$ Pa (stabilized) and $G_0 = 0.0218$ Pa (fresh); only a slight difference. The tangent moduli K' do show some deviation. The stabilized sample exhibits a higher frequency of intertio-elastic oscillations, indicating a larger tangent modulus $K' = 0.0435$ Pa, compared to $K' = 0.0291$ Pa for the fresh sample. For both stabilized and fresh samples we observe that the tangent modulus is larger than the secant modulus, $K' > G_0$. As such, the hagfish slime creep response is non-linear and locally strain stiffening even at this small imposed stress $\sigma_0 = 0.01$ Pa.

3. Constitutive network theory

The observed non-linear rheological features of hagfish slime (to be described in more detail in Section 5), combined with the current understanding of hagfish slime components, are suggestive of a microstructural constitutive model based on network theory. The hagfish slime network is composed of threads (consisting of packed intermediate filaments, or IFs) and mucus. There has been recent progress in modeling IFs from the molecular scale upward, e.g. [17,18], as well as networks of single IFs, e.g. [19]. Hagfish slime has additional hierarchy in that the IFs are packed into threads, and these threads interact with mucus components to form the final network. Here we develop a mesoscale model for this composite network while considering the experimentally observed non-linear viscoelastic response.

One particularly striking feature of the non-linear mechanical response is that the tangent modulus is larger than the secant

modulus (Fig. 2). Furthermore, as will be shown in Figs. 5 and 6, the secant elastic modulus strain-softens in response to increasing load, yet the local tangent elastic modulus strain-stiffens. This juxtaposition of simultaneous softening and stiffening suggests a network structure composed of non-linear elastic strain-stiffening elements in which the overall structure can experience softening as elements are stretched and network junctions are destroyed. One may picture this by considering the slime to be made up of non-linear elastic elements that are held together by weak cross-links. Such a network may strain soften as cross-links break or relax (as measured by the secant modulus G_0). For sufficiently large deformation, the response to small oscillatory strain about a non-zero mean strain can be dominated by the non-linear elastic elements (and not the cross-link relaxation). In this non-linear regime the local tangent modulus K' will be dominated by the non-linear strain-stiffening elastic elements, and K' may therefore exhibit strain-stiffening.

This proposed relation of microstructure to rheology is developed by considering a suitable rheological constitutive equation based on these microstructural concepts. A successful model will explain the observed features, yet have low complexity in order to minimize the number of material parameters to be fitted.

The hagfish slime is modeled as a transient network of connected elastic elements in the presence of a Newtonian background fluid. We idealize the total macroscopic stress tensor $\boldsymbol{\pi}$ as a superposition of the elastic network and solvent,

$$\boldsymbol{\pi} = \boldsymbol{\pi}^E + \boldsymbol{\pi}^S \tag{1}$$

where $\boldsymbol{\pi}^E$ is the stress from the elastic network and $\boldsymbol{\pi}^S$ is the stress from the solvent. The solvent stress is given by

$$\boldsymbol{\pi}^S = \eta_s \dot{\boldsymbol{\gamma}} \tag{2}$$

where η_s is the solvent viscosity and $\dot{\boldsymbol{\gamma}}$ is the rate of deformation tensor, defined as $\dot{\boldsymbol{\gamma}} = \nabla \boldsymbol{v} + (\nabla \boldsymbol{v})^T$ where $\boldsymbol{v}$ is the local fluid velocity vector.

The elastic stress tensor $\boldsymbol{\pi}^E$ will derive from an idealized affinely deforming network of elastic elements. The fundamental principles of network models are outlined by Bird et al. [20]. A variety of non-linear viscoelastic network models exist [21–26]. The model developed here is most similar to that of Ng et al. [27], with modifications to account for the softening of the *secant* elastic modulus and simultaneous stiffening of the *tangent* elastic modulus which we report here for hagfish slime. We first construct the relationship between the macroscopic stress $\boldsymbol{\pi}^E$ and the microstructural state. The orientation and extension of an elastic element is represented by the end-to-end vector $\boldsymbol{Q}$, and each element carries a force $\boldsymbol{F}$ along its length. The macroscopic elastic stress tensor $\boldsymbol{\pi}^E$ resulting from an ensemble of such elastic elements with number density n is

$$\boldsymbol{\pi}^E = n \langle \boldsymbol{QF} \rangle \tag{3}$$

where $\langle \rangle$ denotes the ensemble average of the distribution. Here we have assumed a single species of elastic elements which will eventually lead to a single viscoelastic relaxation time. This choice of a single relaxation time is reasonable for our range of experimental data (see Fig. 4a, $0.1\ \text{rad s}^{-1} \leq \omega \leq 10\ \text{rad s}^{-1}$), but the model could be made more general by considering a superposition of multiple species, $\boldsymbol{\pi}^E = \Sigma \boldsymbol{\pi}_k^E$, with a distribution of relaxation times λ_k [27]. We will model the elastic elements as purely elastic (no dissipation), but we note that hagfish threads [10], and their intermediate filament components [17], are dissipative at sufficiently large strains. Intra-thread dissipation would originate from the α–helix to β–sheet transition of the intermediate filament proteins or relative sliding of intermediate filaments, and these mechanisms have been identified even from molecular simulations [17], which also show a response dependent on pulling speed.

We consider intra-thread dissipation a higher order effect and do not include this in our model because such dissipation typically requires very large strains after the threads have been straightened and aligned. We therefore model the elastic force $\boldsymbol{F}$ as a non-linear purely elastic spring, e.g. from the straightening of the threads,

$$\boldsymbol{F} = Hf(Q)\boldsymbol{Q} \tag{4}$$

where H is the linear Hookean spring constant and $f(Q)$ is a dimensionless non-linear multiplicative factor in which $f_{eq} = 1$ at equilibrium. We will choose a non-linearity of the FENE (finitely extensible non-linear elastic) form, for which the force diverges as an elastic element is stretched to a maximum allowable length. With this formulation $f(Q)$ provides non-linear elastic stiffening. We substitute Eq. (4) into Eq. (3) and use a simplifying closure approximation of the FENE-P form, $\langle f(Q)\boldsymbol{QQ} \rangle = f(Q)\langle \boldsymbol{QQ} \rangle$, giving

$$\boldsymbol{\pi}^E = nHf(Q)\langle \boldsymbol{QQ} \rangle. \tag{5}$$

We will rewrite the quantity $\langle \boldsymbol{QQ} \rangle$ by introducing a dimensionless microstructural tensor $\boldsymbol{A}$,

$$\boldsymbol{A} \equiv \frac{\langle \boldsymbol{QQ} \rangle}{Q_{eq}^2} \tag{6}$$

where $Q_{eq}^2 = \text{Tr}\langle \boldsymbol{QQ} \rangle_{eq}$ is the mean square length of the segments at equilibrium and Tr denotes the trace of the tensor. At equilibrium the microstructural tensor becomes $\boldsymbol{A}_{eq} = \boldsymbol{I}$.

We furthermore introduce instantaneous elastic softening of the network due to the loss of network connections during stretch. The loss of junctions will decrease the number density of elastic elements, n, which contribute to the elastic stress. We model this as instantaneous loss corresponding to the microstructural stretch state,

$$n = n_0 g(\boldsymbol{A}) \tag{7}$$

where n_0 is the equilibrium number density and $g(\boldsymbol{A})$ is a decreasing function of a scalar invariant of $\boldsymbol{A}$ for which $g_{eq} = 1$ at equilibrium. We will similarly represent the stiffening factor in terms of a scalar invariant of the microstructural tensor, $f(\boldsymbol{A})$. Before choosing explicit functional forms of $f(\boldsymbol{A})$ and $g(\boldsymbol{A})$, we can write the general expression relating the macroscopic network stress $\boldsymbol{\pi}^E$ to the microstructural state of stretch, $\boldsymbol{A}$. Combining Eqs. (5)–(7) gives

$$\boldsymbol{\pi}^E = Gg(\boldsymbol{A})f(\boldsymbol{A})\boldsymbol{A} \tag{8}$$

where we have defined a macroscopic elastic modulus as $G \equiv n_0 H Q_{eq}^2$. Eq. (8) includes an isotropic pressure at equilibrium. We remove this by considering the extra stress tensor, and write the total extra stress tensor as a superposition of the elastic network (Eq. (8)) and the background solvent (Eq. (2))

$$\boldsymbol{\sigma} \equiv \boldsymbol{\pi} - \boldsymbol{\pi}_{eq} \tag{9}$$

$$= G[g(\boldsymbol{A})f(\boldsymbol{A})\boldsymbol{A} - \boldsymbol{I}] + \eta_s \dot{\boldsymbol{\gamma}}. \tag{10}$$

In this formulation the multiplicative combination $g(\boldsymbol{A})f(\boldsymbol{A})$ appears as an effective non-linear elastic spring force. The functional forms of the instantaneous softening term $g(\boldsymbol{A})$ and the stiffening FENE spring term $f(\boldsymbol{A})$ will be written as a function of a scalar invariant of the tensor $\boldsymbol{A}$. We will use the quantity $[\text{Tr}(\boldsymbol{A})-3]$ as a scalar to represent the microstructural state, which is equal to zero at equilibrium since $\boldsymbol{A}_{eq} = \boldsymbol{I}$. For the softening function $g(\boldsymbol{A})$ we choose the empirical expression

$$g(\boldsymbol{A}) = \exp\{-\alpha[\text{Tr}(\boldsymbol{A})-3]\} \tag{11}$$

where α is a dimensionless softening parameter. For the FENE spring we choose a commonly used force law

$$f(\boldsymbol{A}) = \frac{1}{1-[\text{Tr}(\boldsymbol{A})-3]/b} \tag{12}$$

where b is the finite extensibility parameter and represents the maximum allowable stretch in the element. The elastic force stiffens and diverges as $[\text{Tr}(\boldsymbol{A})-3] \rightarrow b$. A linear Hookean spring is obtained in the limit that $b \rightarrow \infty$.

Eqs. (10)–(12) are used to calculate the instantaneous macroscopic stress as a function of the microstructural tensor $\boldsymbol{A}$. The tensor $\boldsymbol{A}$ must still be related to the macroscopic deformation. Here we select an evolution equation which introduces transient viscoelastic relaxation. We consider a network in which junctions are continuously destroyed at a rate $1/\lambda(\boldsymbol{A})$, and are created at a constant rate $1/\lambda_0$. In this way the viscoelastic effects come from the transient nature of weak cross-link connections between the threads and mucin-like molecules, and the elastic elements of the network are themselves considered as purely elastic. In our network model, time-dependent properties originate only from the loss and creation of network connections, and the evolution equation for the microstructural tensor $\boldsymbol{A}$ is given by

$$\boldsymbol{A}_{(1)} = \frac{1}{\lambda_0}\boldsymbol{I} - \frac{1}{\lambda(\boldsymbol{A})}\boldsymbol{A} \qquad (13)$$

where the subscript (1) indicates the upper convected time derivative, $\boldsymbol{A}_{(1)} \equiv d(\boldsymbol{A})/dt + (\boldsymbol{v} \cdot \nabla)\boldsymbol{A} - (\nabla \boldsymbol{v})^T \cdot \boldsymbol{A} - \boldsymbol{A} \cdot (\nabla \boldsymbol{v})$. A purely elastic network would result if the creation and loss rates were set to zero, for which Eq. (13) becomes $\boldsymbol{A}_{(1)}=0$. For this purely elastic case the tensor $\boldsymbol{A}$ would be advected by the macroscopic deformation via the velocity gradient terms contained in the upper convected derivative. Furthermore, for $\boldsymbol{A}_{(1)}=0$, viscoelastic relaxation is non-existent, and the stress is an instantaneous non-linear function of $\boldsymbol{A}$ via Eq. (10); recall that $g(\boldsymbol{A})$ and $f(\boldsymbol{A})$, Eqs. (11) and (12), are instantaneous functions of $\boldsymbol{A}$ and therefore cannot capture time-dependent viscoelastic relaxation, only elastic softening or stiffening. Finite rates of loss $1/\lambda(\boldsymbol{A})$ and creation $1/\lambda_0$ enable viscoelastic transient stress relaxation and growth. The loss and destruction rates must be identical at equilibrium, but we model the rate of destruction as an increasing function of the microstructural stretch. We consider a destruction rate which is related to the force carried in the connecting elastic fibers, and therefore choose the FENE function $f(\boldsymbol{A})$ (Eq. (12)) as the multiplicative factor for the destruction rate,

$$\frac{1}{\lambda(\boldsymbol{A})} = \frac{1}{\lambda_0}f(\boldsymbol{A}). \qquad (14)$$

This choice allows for the same non-linear parameter b to govern both the elastic stiffening and non-linear viscoelastic relaxation. We remark that this is a simplified version of the non-linear loss rate used by Ng et al. [27]. Ng et al. include an additional multiplicative factor for the loss rate $1/\lambda(\boldsymbol{A})$ which linearly increases as a function of $[\text{Tr}(\boldsymbol{A})-3]$. Additionally, they use a parameter to shift the finite extensibility parameter b used for the loss rate dependence (Eq. (14)) to be different than that used for the stress calculation (Eq. (10)). Here we have pursued a minimalist model which can reveal the qualitative non-linear behavior of hagfish slime with a minimum number of parameters.

The final model is represented by Eqs. (10)–(14), which requires three linear viscoelastic parameters: the polymeric elastic modulus G, the polymeric relaxation time λ_0, and the solvent viscosity η_s. Additionally, two non-linear parameters are required: the finite extensibility parameter b and the instantaneous elastic softening parameter α. In the linear viscoelastic limit ($\alpha=0, b \rightarrow \infty$) the model is identical to the upper convected Jeffreys model (also known as Oldroyd-B) [28]. The inclusion of FENE springs via $f(\boldsymbol{A})$ (Eq. (12), $b=$ finite) will introduce elastic strain-stiffening via Eq. (10), and non-linear relaxation mechanisms (e.g. shear-thinning) via Eq. (13). Elastic softening is introduced by the softening factor $g(\boldsymbol{A})$ for finite $\alpha > 0$ (Eq. (11)).

4. Calculations

4.1. Simulation of the network model

The constitutive model (Eqs. (10)–(14)) is simulated for homogeneous simple shear deformations, neglecting the inertia of the material sample but including the rotational inertia of the instrument. The material stress tensor $\boldsymbol{\sigma}$ is homogeneous and only a function of time under these assumptions.

For simulations with controlled shear-rate deformation $\dot{\gamma}_{12}(t)$, e.g. oscillatory shear with $\dot{\gamma}_{12}(t)=\gamma_0\omega\cos(\omega t)$, the evolution equations for the components of $\boldsymbol{A}$ (Eq. (13)) can be solved explicitly, resulting in a system of coupled first order ordinary differential equations with non-constant coefficients. The solution is obtained numerically using an ODE solver in MATLAB with a variable time stepper. The resulting time-dependent microstructural tensor $\boldsymbol{A}$ is then used to calculate the material stress via Eq. (10).

For simulations of load-controlled tests, e.g. creep tests, one must solve the evolution equations for $\boldsymbol{A}$ simultaneously with an equation representing the imposed stress. The imposed *material* stress may be different than the apparent imposed instrument stress owing to the rotational inertia of the instrument. Although the rotational inertia of the sample is neglected, we do consider the rotational inertia of the instrument for load-control tests. It is this instrument inertia which causes the inertio-elastic ringing observed in Figs. 2 and 5, as mentioned in Section 2.1. The resulting equation of motion is derived from the angular momentum (torque) balance around the rotational instrument, and arranged to relate the apparent imposed shear stress σ_0 to the material shear stress σ_{12}. For a creep test (step torque loading) the equation of motion takes the general form:

$$\frac{I}{c}\ddot{\gamma}_{12}(t) = H(t)\sigma_0 - \sigma_{12}(t) \qquad (15)$$

where I is the moment of inertia of the rotating instrument components, $H(t)$ is the Heaviside step function characterizing the imposition of the apparent instrument stress (torque) and $\sigma_{12}(t)$ is the true shear stress in the sample arising from deformation. In this expression c is a geometry factor given by $\gamma_{12}/\sigma_{12}=c\phi/T$ that relates the raw (or measured) angular displacement ϕ and torque T to the rheological quantities of interest, i.e. shear strain γ_{12} and stress σ_{12} (i.e. $c=F_\gamma/F_\sigma$ where $\sigma_{12}=F_\sigma T$ and $\gamma_{12}=F_\gamma\phi$). For all of our experiments $I/c=2.9465 \times 10^{-2}$ kg/m.

It is immediately apparent that the sample stress is not a step function, $\sigma_{12}(t) \neq H(t)\sigma_0$, due to the finite inertia of any real rheometric instrument, although it eventually reaches the constant, desired value after the inertial transient has decayed. The stress calculator for $\sigma_{12}(\boldsymbol{A})$ (Eq. (10)) is substituted into Eq. (15) and the resulting expression arranged as a first order ordinary differential equation explicit in $d(\dot{\gamma}_{12})/dt$

$$\frac{d}{dt}\dot{\gamma}_{12} = \frac{c}{I}[H(t)\sigma_0 - Gg(\boldsymbol{A})f(\boldsymbol{A})A_{yx} - \eta_s\dot{\gamma}_{12}]. \qquad (16)$$

For the step torque (creep) tests, Eq. (16) is used as an additional coupled ODE and solved simultaneously with the evolution equations for the components of $\boldsymbol{A}$, Eq. (13). The initial conditions used are $\boldsymbol{A}(t=0)=\boldsymbol{I}$, with $\dot{\gamma}_{12}(t=0)=0$ for imposed stress simulations.

4.2. Inertio-elastic ringing analysis

As noted in Section 2.1, the inertio-elastic ringing artifacts present in the creep tests will be deliberately utilized for non-linear rheological analysis. By measuring the ringing frequency ω_* and the logarithmic decrement Δ associated with the ringing, Struik [13] showed that the viscoelastic moduli can be approximated for small Δ, negligible instrument elasticity, and negligible sample

inertia by the following expressions:

$$K' \approx \frac{I\omega_*^2}{c}(1+(\Delta/2\pi)^2) \tag{17}$$

$$K'' \approx \frac{I\omega_*^2}{c}\left(\frac{\Delta}{\pi}\right) \tag{18}$$

where ω_* is the ringing frequency and Δ is the logarithmic decrement. Here we use the notation K' and K'' to mean the tangent (or differential) moduli, since the ringing oscillations occur about an imposed stress which may be in the non-linear regime and therefore represent the local, tangent material response, e.g. $K' \sim d\sigma_{12}/d\gamma_{12}$ [15].

We calculate the values of ω_* and Δ from the apparent compliance $J(t) = \gamma(t)/\sigma_0$ by assuming a prototypical Maxwell response superimposed with decaying oscillations,

$$J(t) = X\exp\left(-\Delta\frac{\omega_* t}{2\pi}\right)\sin(\omega_* t + \Psi) + Y + Zt \tag{19}$$
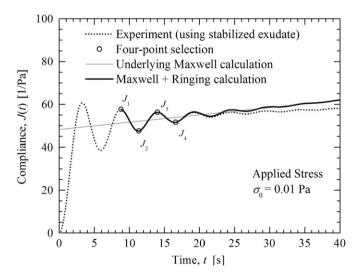
in which X is the ringing amplitude, Y is the initial compliance, Z is the fluidity, and Ψ is an arbitrary phase. The form of Eq. (19) allows for an estimate of the instantaneous secant elastic modulus, $G_0 = 1/Y$, which will be compared to the tangent elastic modulus K' to identify material non-linearity.

Identifying four successive peak/valley data points from the experimental data, $t_1 \rightarrow t_4$ and $J_1 \rightarrow J_4$, provides sufficient information to determine all of the parameters of interest [14] (visualized in Fig. 3). The ideal time spacing forces the following relationships of the time points, $t_2 = t_1 + \pi/\omega$, $t_3 = t_1 + 2\pi/\omega$, and $t_4 = t_1 + 3\pi/\omega$. These four data points then provide the following system of equations with the assumed underlying model (using Eq. (19)):

$$J_1 = X\exp\left(-\Delta\frac{\omega_* t_1}{2\pi}\right)(+1) + Y + Zt_1 \tag{20}$$

$$J_2 = X\exp\left(-\Delta\frac{\omega_* t_1 + \pi}{2\pi}\right)(-1) + Y + Z(t_1 + \pi/\omega_*) \tag{21}$$

$$J_3 = X\exp\left(-\Delta\frac{\omega_* t_1 + 2\pi}{2\pi}\right)(+1) + Y + Z(t_1 + 2\pi/\omega_*) \tag{22}$$

Fig. 3. Calculation method for inertio-elastic ringing analysis demonstrated with the hagfish slime data of Fig. 2 (stabilized exudate). Four points, J_1–J_4, are identified at successive peaks and valleys to fit a Maxwell response superimposed with decaying oscillations (Eq. (19)). Here the calculation yields $J_0 = 48.3$ Pa^{-1} ($G_0 = 1/J_0 = 0.0207$ Pa), $\eta_0 = 2.92$ Pa s, $\omega_* = 1.21$ rad s^{-1}, $\Delta = 0.669$, and $K' = 0.0435$ Pa. At longer times the assumption of a negligible retardation time breaks down as the rate of deformation $\dot{\gamma}(t) = \dot{J}(t)\sigma_0$ decreases and deviates from the idealized behavior.

$$J_4 = X\exp\left(-\Delta\frac{\omega_* t_1 + 3\pi}{2\pi}\right)(-1) + Y + Z(t_1 + 3\pi/\omega_*). \tag{23}$$

The inertio-elastic ringing frequency is calculated from the total time-span of the data points covering 1.5 periods,

$$\omega_* = \frac{2\pi}{t_4 - t_1} 1.5. \tag{24}$$

The logarithmic decrement, Δ, can be determined through a proper elimination of the variables X, Y, and Z. Two independent methods of eliminating Y and Z are used, namely $J_1 + J_3 - 2J_2$, and $-J_2 - J_4 + 2J_3$. The ratio of these two terms further eliminates X and allows for Δ to be calculated as a function of the four point $J_1 \rightarrow J_4$. This resulting expression is
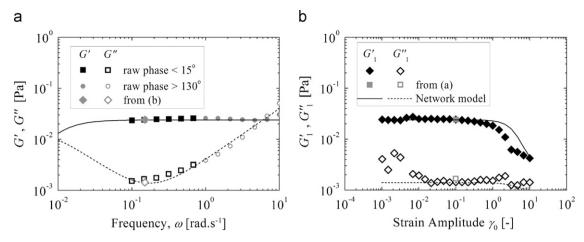
$$\Delta = 2\ln\left(\frac{J_1 - 2J_2 + J_3}{-J_2 + 2J_3 - J_4}\right). \tag{25}$$

Using the values of ω_* and Δ, the tangent moduli K' and K'' can be estimated via Eqs. (17) and (18). The system of equations fully constrains the values of the remaining unknowns X, Y, Z, and Ψ.

5. Results and discussion

The results presented here are the first tests to use a well-defined deformation field to characterize the intrinsic non-linear rheological properties of a hagfish slime network. The same "fresh" sample used for the creep tests of Fig. 2 was also used for a linear viscoelastic frequency sweep (Fig. 4a) and a non-linear amplitude sweep, often referred to as large amplitude oscillatory shear (LAOS) (Fig. 4b). The hagfish slime sample is so soft that inertia easily dominates the response. The predominant role of inertia is indicated by the raw phase angle between the torque and displacement oscillations. A purely material response will have a phase angle less than or equal to 90°, but here we observe a phase angle greater than 130° for sufficiently high frequency. This critical frequency for which inertial effects are comparable to material resistance corresponds to the inertio-elastic ringing frequency shown in Fig. 2, $\omega_* = 0.99$ rad s^{-1}. With such large raw phase angles the rotational inertia of the instrument dominates the response, and a large inertia correction must be made to the data. Data points with large inertia corrections are distinguished as gray circles in Fig. 4a. Frequencies up to nearly $\omega = 10$ rad s^{-1} still give reasonable results after the inertial corrections.

The simple network theory of Section 3, with a single linear viscoelastic relaxation time of the network λ_0, corresponds well with the experimental measurements. The linear viscoelastic model response is shown as lines in Fig. 4a. In the linear viscoelastic regime only three model parameters can be specified: the network elastic modulus $G = 0.024$ Pa, network relaxation time $\lambda_0 = 200$ s, and solvent viscosity $\eta_s = 0.004$ Pa s. At high frequency the elastic modulus plateaus to a constant value $G = 0.024$ Pa, and the loss modulus increases with frequency due to the solvent viscosity $G'' \sim \eta_s\omega$. The value of solvent viscosity, $\eta_s = 0.004$ Pa s is slightly larger than water ($\eta = 0.001$ Pa s), owing to mucus or thread components that are not bound to the network. The choice of solvent viscosity $\eta_s = 0.004$ Pa s is further validated by viscosity measurements of hagfish mucin solutions [8], which exhibit a viscosity close to that of seawater. The low frequency behavior is determined by the relaxation time $\lambda_0 = 200$ s. This value of λ_0 is chosen to reasonably capture the flow observed in creep tests and also the value of G'' at $\omega = 0.15$ rad s^{-1} since this frequency was probed in more detail with a sweep in amplitude γ_0. A relaxation time on the order of hundreds of seconds was also reported by Fudge et al. for whole slime [8]. The similar relaxation time is noteworthy, considering that large deformation and a complex deformation field were used in [8], whereas here we use a simple
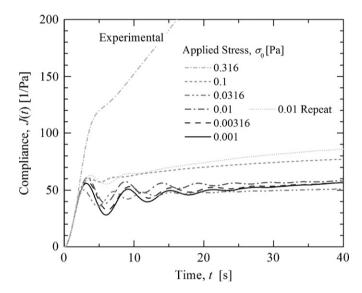
Fig. 4. Oscillatory shear experiments with hagfish slime reconstituted from fresh exudate, shown with the network model response (lines) with parameters $G=0.024$ Pa, $\lambda_0=200$ s, $\eta_s=0.004$ Pa s, $b=60$, and $\alpha=1/22$. (a) Linear viscoelastic frequency sweep with prescribed strain amplitude $\gamma_0=10\%$. The mechanical resistance is so low ($G'<0.03$ Pa) that inertial effects from the rheometer spindle must be removed; strong inertial effects are evidenced by a sharp jump in the raw phase angle $\delta=14.7-134.9°$ at $\omega=1$ rad s^{-1}, corresponding to the resonant frequency of the material–instrument system $\omega_*\approx 1$ rad s^{-1} (Fig. 2). (b) Non-linear amplitude sweep at fixed frequency $\omega=0.15$ rad s^{-1}; at large amplitudes the average elastic modulus G'_1 softens with increasing strain amplitude γ_0.

shear deformation in the linear viscoelastic regime. The linear viscoelastic moduli for this sample show weak frequency dependence, and the value of $G'=0.024$ Pa corresponds well with the results of the creep test of Fig. 2 for which $G_0=0.0218$ Pa at $\sigma_0=0.01$ Pa. Note that this stress imposed for the creep test is already in the non-linear regime since $K'\neq G_0$ (Fig. 2), but the frequency sweep of Fig. 4a is in the linear viscoelastic regime. The lower modulus of the non-linear creep test is consistent with softening of the secant elastic modulus G_0, which we can observe here with the non-linear oscillatory shear test (Fig. 4b).

A non-linear oscillatory shear test with increasing amplitude γ_0 was conducted at imposed frequency $\omega=0.15$ rad s^{-1}, Fig. 4b. Here the steady oscillatory behavior is characterized by the first-harmonic elastic modulus G'_1 and first-harmonic viscous modulus G''_1. For a strain amplitude sweep, the linear viscoelastic regime exists at small values of strain amplitude γ_0. The experimental results plateau to linear viscoelastic values for small strain amplitude γ_0, but at the very small strain $\gamma_0=0.001$ the torque amplitude response is extremely low, $T_0=1.3\ 10^{-9}$ N m, and the measured values become noisy. This is especially true for the subdominant component G''_1 at small strain amplitude.

As the strain amplitude increases into the non-linear viscoelastic regime, the elastic modulus decreases, indicating an overall softening of the network with increased strain amplitude. Fig. 4b shows that the hagfish slime network degrades above a critical strain amplitude $\gamma_0\approx 1$, which corresponds to a stress amplitude $\sigma_0\approx G'\gamma_0=0.024$ Pa. No stiffening is apparent from the first-harmonic measure of elastic modulus G'_1; instead G'_1 only softens with increased amplitude.

The network model response to large amplitude oscillatory shear (LAOS) was simulated as described in Section 4.1, and characterized by G'_1 and G''_1 as shown in Fig. 4b with the lines. The linear viscoelastic parameters have already been specified, as shown in Fig. 4a. Two non-linear parameters are required for the network model: the finite extensibility parameter $b=60$, and the elastic softening parameter $\alpha=1/22$. These values are chosen in order for the model to best correspond with both LAOS tests (Fig. 4b) and non-linear creep tests (Figs. 5 and 6). The choice of $b=60$ is reasonable, as typical polymeric materials generally exhibit a range of values from $30<b<300$ [29]. The value of the softening parameter $\alpha=1/22$ is sufficiently strong that the effective multiplicative spring constant $g(\boldsymbol{A})f(\boldsymbol{A})$ will initially soften, but is weak enough that the stiffening of finite extensibility can still be observed at larger microstructural stretch. The inclusion of these
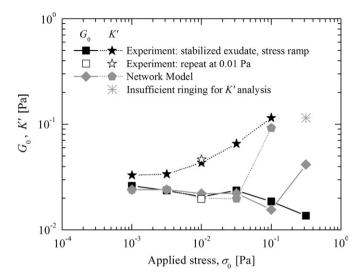

Fig. 5. Experimental creep tests in shear conducted with hagfish slime reconstituted from stabilized exudate. The minimum imposed shear stress $\sigma_0=0.001$ Pa corresponds to a rotational torque $T=0.055$ μN m which was the lowest load that provided a meaningful measurement. The non-linear time-dependent creep response is examined at increasing stress amplitudes, followed by a repeat test at $\sigma_0=0.01$ Pa to examine reversibility.

two non-linear parameters, $b=60$ and $\alpha=1/22$, give the correct trend and a reasonable fit to the first-harmonic viscoelastic moduli $G'_1(\gamma_0)$ and $G''_1(\gamma_0)$ at the imposed frequency $\omega=0.15$ rad s^{-1}, as shown by the lines in Fig. 4b.

Local elastic stiffening may still exist behind the overall softening of $G'_1(\gamma_0)$, e.g. the large strain amplitude puts the network in a state with non-linear elasticity but with an overall decrease in modulus (e.g. as included with the network model of Section 3). It is typically possible to examine the resulting LAOS stress signal to probe for local elastic stiffening in the presence of overall softening [30]. However, for this extremely soft material the experimental torque response is so low that noise in the oscillatory signal obscures any higher order non-linear features. We will therefore utilize non-linear creep tests to examine higher order stiffening via the tangent modulus calculation.

Creep tests were performed over a range of input stress amplitude to better explore the non-linear viscoelastic behavior

Fig. 6. Inertio-elastic analysis of experimental and network model creep tests in shear. The original transient compliance curves are presented in Fig. 5 for the experiments and in Fig. 7 for the network model simulation. The elastic analysis of each curve includes the tangent modulus K' (Eq. (17)) and initial secant modulus G_0 (Eq. (19)). The network model captures the simultaneous softening of G_0 and stiffening of K'_0 as the model enters the non-linear viscoelastic regime.

of hagfish slime networks using the torque-controlled rheometer (Fig. 5). Stabilized slime was used for these creep tests. Note that the creep response of the stabilized slime (at $\sigma_0 = 0.01$ Pa) corresponded well with the fresh slime creep response, as shown in Fig. 2. This gives confidence that the stabilized slime exudate can be used in place of fresh exudate, and therefore future research can avoid the maintenance and care of hagfish at multiple sites.
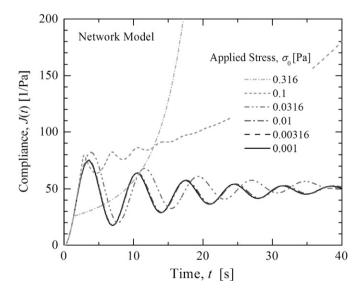
As shown in Fig. 5, the slime network responds as a predominantly elastic material for sufficiently small values of stress. The compliance quickly grows, undergoes inertio-elastic oscillations, and thereafter grows at a slow rate with $\eta \approx 2.6$ Pa s. The predominantly elastic creep response is consistent with the LAOS test in Fig. 4b which shows $G'_1 \gg G''_1$ in the small strain region. The material softens at larger stresses as indicated by an increase in the initial compliance J_0, which can be considered equivalently as a softening of the initial secant elastic modulus $G_0 = 1/J_0$. The softening is visually apparent near $\sigma_0 = 0.1$ Pa, which is a slightly larger stress than observed in Fig. 4b in which softening initiates near $\sigma_0 = 0.024$ Pa. In addition to softening, the sample eventually yields and flows (shear-thinning viscosity) at large imposed stress, e.g. at $\sigma_0 = 0.316$ Pa in which $\eta \approx 0.13$ Pa s. Inertio-elastic ringing is observed in all of these tests, and was used for analysis of each curve except $\sigma_0 = 0.316$ Pa which had insufficient ringing information available.

The ringing analysis of the creep curves results in stress amplitude dependent values of the secant modulus $G_0(\sigma_0)$ and tangent modulus $K'(\sigma_0)$, which are both given in Fig. 6. At sufficiently small stress, the values of G_0 and K' would be expected to converge, and indeed this is approximately the case for the measured data here. As stress amplitude is increased, the values diverge. The secant modulus G_0 is initially constant and eventually decreases, which qualitatively corresponds to the LAOS results of softening first-harmonic elastic modulus $G'_1(\gamma_0)$ (Fig. 4b). The non-linear behavior is quite rich as the tangent modulus is larger than the secant modulus for all tests, and increases as a function of stress amplitude indicating non-linear elastic stiffening of the tangent modulus. The elasticity stiffens by about one order of magnitude before the sample response is dominated by flow and the tangent modulus can no longer be measured.

After conducting the creep tests at increasing stress, a repeat test was performed at a stress $\sigma_0 = 0.01$ Pa. The resulting transient compliance $J(t)$ is higher than the original curve at the same stress $\sigma_0 = 0.01$ Pa, especially when shown on axes with linear scales. However, the sample predominantly recovers the elastic properties as shown by a similar flow viscosity upon repeat ($\eta \approx 2.2$ Pa s) and comparable values of G_0 and K' in Fig. 6. That the material is approximately reversible within this range of stress is encouraging for the network model, which by construction is reversible.

The network model was simulated in a creep test, including instrument inertia effects, as outlined in Section 4.1. The same model parameters are used as for the oscillatory shear simulations (Fig. 4), i.e. $G = 0.024$ Pa, $\lambda_0 = 200$ s, $\eta_s = 0.004$ Pa s, $b = 60$, $\alpha = 1/22$. The simulated transient compliance $J(t)$ is given in Fig. 7 for the same range of stresses used in the experimental measurements of Fig. 5. The inertio-elastic oscillations are immediately apparent in the simulation. The oscillations are analyzed in the same way as the experimental data using the four-point method (Fig. 3), and the resulting values of secant modulus G_0 and tangent modulus K' are shown in Fig. 6.

The model captures the initial trend of the non-linear behavior. Specifically, it captures the stiffening of the tangent modulus K' which corresponds to increased inertio-elastic ringing frequency, e.g. at $\sigma_0 = 0.1$ Pa. It simultaneously captures the softening of the secant modulus G_0, e.g. at $\sigma_0 = 0.1$ Pa, which can be visualized in the transient creep tests of Fig. 7 as an increase in the initial compliance J_0.

There are two features which are not precisely captured by this minimalist constitutive model. The first is that experimental measurements suggest a more gradual stiffening of the tangent modulus $K'(\sigma_0)$ than provided by the model (see comparison in Fig. 6). Secondly, the experimental measurements show an ever-decreasing initial secant modulus G_0 (increasing initial compliance J_0) for this range of stress amplitude, whereas the model predicts the trend of decreasing secant modulus G_0 initially but eventually deviates and shows an increase in the secant modulus G_0 at the largest imposed stress $\sigma_0 = 0.316$ Pa, Fig. 6. This can be visualized in the simulation shown in Fig. 7 at $\sigma_0 = 0.316$ Pa by the *decrease* in the initial compliance J_0, corresponding to a stiffening of $G_0(\sigma_0) = 1/J_0(\sigma_0)$. If the softening term were to be eliminated ($\alpha = 0, g(A) = 1$), then the initial elastic modulus G_0 would only

Fig. 7. Simulation of shear creep tests using the network theory constitutive model. The inertio-elastic ringing is apparent due to the inclusion of instrument inertia in the simulation—such ringing is not inherently contained in the constitutive model. The model parameters are $G = 0.024$ Pa, $\lambda_0 = 200$ s, $\eta_s = 0.04$ Pa s, $b = 60$, $\alpha = 1/22$.

be an increasing function of imposed stress σ_0, as governed by the finite extensible stiffening elastic elements. Eventual long-time softening can be obtained for $g(\boldsymbol{A}) = 1$ due to non-linear relaxation mechanisms, but softening of the instantaneous elastic modulus G_0 would not be obtained for $g(\boldsymbol{A}) = 1$. The inclusion of a non-trivial instantaneous softening term $g(\boldsymbol{A})$ introduces softening of the initial modulus $G_0(\sigma_0)$ for intermediate stresses, but eventually the dramatic stiffening of the parameter $f(\boldsymbol{A})$ dominates and forces G_0 to increase. The deviations between model and experiment suggest that the simple softening term may be modified to include transient or irreversible destruction, which could depend on the maximum stretch experienced by the network rather than the instantaneous microstructural state, as implemented here. A more precise and complex model might also include a different non-linear spring law $f(\boldsymbol{A})$, such as the wormlike chain model [31], entropic elasticity of semiflexible elements [32], or a coarse-grained empirical function which matches the experimentally measured non-linear elastic force–stretch curve of hagfish threads. Mucin vesicles may also contribute to network elasticity. Recent work has shown that some of the mucin vesicles form very soft elastic strands during slime deployment [9]. Incorporating multiple network elements into the model (e.g. for threads and mucins) may therefore improve the fit to empirical measurements.

The strength of the model is the distinct ability to capture simultaneous softening of $G'_1(\gamma_0)$ and $G_0(\sigma_0)$ and stiffening of $K'(\sigma_0)$. Other network models can capture long time, steady state softening in concert with local stiffening, but not the *instantaneous* softening of G_0. For example, the model of Ng et al. [27] can capture long-time steady state oscillatory softening of $G'_1(\gamma_0)$, but despite the inclusion of a more complicated junction loss rate term, $1/\lambda(\boldsymbol{A})$, it fails to allow softening of the initial secant elastic modulus at short timescales. Our experimentally observed softening of the initial secant modulus G_0 (Figs. 5 and 6) has motivated the introduction of the network model used here and will serve as a guidepost for the further refinement of constitutive models for biological elastic networks such as hagfish slime.

6. Conclusions

These tests represent the first reported intrinsic property measurement of hagfish slime with a well-defined deformation field (simple shear), and include both linear and non-linear rheological responses. The measurement of intrinsic material functions has enabled us to develop a constitutive model based on the mesoscopic structure–property relationships of a transient network model.

The fresh and stabilized slime exudate have comparable mechanical properties, especially as indicated by the initial secant elastic modulus $G_0 \approx 0.02$ Pa for each. This elastic modulus is so soft that careful rheological measurements must be performed, since instrument inertia contributes artifacts to the measured response. We demonstrate that appropriately considering the raw oscillatory data, in the context of inertio-elastic ringing, can allow for accurate non-linear characterization of this ultra-soft material. In the context of advanced rheometry methods, the hagfish slime network is yet another example of the fact that the typical first-harmonic analysis of LAOS tests (Fig. 4b) can be insufficient to describe the true non-linear viscoelastic material response. Here we observe elastic strain-stiffening, which is revealed by the tangent modulus analysis of inertio-elastic ringing (Fig. 5b).

We have developed a microstructural network model which can describe the qualitative non-linear viscoelastic features measured here, in particular the simultaneous softening of the secant modulus and stiffening of the tangent modulus. The softening of the secant modulus corresponds to the breaking of junctions; in the slime this softening corresponds to the loss of weak cross-links that link the slime threads and mucins together. The local strain stiffening of the tangent modulus results from the non-linear elasticity of network components. The slime network components are threads and mucins. It is likely that mucins are strain-stiffening, and it has been shown experimentally that isolated slime threads show extreme strain-stiffening behavior [10]. Simultaneous softening and stiffening have been observed for other biological networks, such as a gluten gel [27], snail pedal mucus [30], and a keratin filament network [33]. The non-linear model developed here has the potential to be more broadly applicable to a variety of biological structures beyond hagfish slime.

References

[1] J.M. Jørgensen, J.P. Lomholt, R.E. Weber, H. Malte, The Biology of Hagfishes, Chapman and Hall, London, New York,, 1998.
[2] S.W. Downing, R.H. Spitzer, E.A. Koch, W.L. Salo, The hagfish slime gland thread cell. 1. A unique cellular-system for the study of intermediate filaments and intermediate filament–microtubule interactions, Journal of Cell Biology 98 (2) (1984) 653–669.
[3] R.H. Spitzer, S.W. Downing, E.A. Koch, W.L. Salo, L.J. Saidel, Hagfish slime gland thread cells. 2. Isolation and characterization of intermediate filament components associated with the thread, Journal of Cell Biology 98 (2) (1984) 670–677.
[4] R.H. Spitzer, E.A. Koch, S.W. Downing, Maturation of hagfish gland thread cell—composition and characterization of intermediate filament polypeptides, Cell Motility and the Cytoskeleton 11 (1) (1988) 31–45.
[5] J. Lim, D.S. Fudge, N. Levy, J.M. Gosline, Hagfish slime ecomechanics: testing the gill-clogging hypothesis, Journal of Experimental Biology 209 (4) (2006) 702–710.
[6] E.A. Koch, R.H. Spitzer, R.B. Pithawalla, D.A.D. Parry, An unusual intermediate filament subunit from the cytoskeletal biopolymer released extracellularly into seawater by the primitive hagfish (*Eptatretus-stouti*), Journal of Cell Science 107 (1994) 3133–3144 part 11.
[7] E.A. Koch, R.H. Spitzer, R.B. Pithawalla, F.A. Castillos, Hagfish biopolymer—a type-I type-II homolog of epidermal keratin intermediate filaments, International Journal of Biological Macromolecules 17 (5) (1995) 283–292.
[8] D.S. Fudge, N. Levy, S. Chiu, J.M. Gosline, Composition, morphology and mechanics of hagfish slime, Journal of Experimental Biology 208 (24) (2005) 4613–4625.
[9] T.M. Winegard, D.S. Fudge, Deployment of hagfish slime thread skeins requires the transmission of mixing forces via mucin strands, Journal of Experimental Biology 213 (8) (2010) 1235–1240.
[10] D.S. Fudge, K.H. Gardner, V.T. Forsyth, C. Riekel, J.M. Gosline, The mechanical properties of hydrated intermediate filaments: insights from hagfish slime threads, Biophysical Journal 85 (3) (2003) 2015–2027.
[11] L.A. Sellers, A. Allen, E.R. Morris, S.B. Rossmurphy, Mechanical characterization and properties of gastrointestinal mucus gel, Biorheology 24 (6) (1987) 615–623.
[12] D.S. Fudge, T. Winegard, R.H. Ewoldt, D. Beriault, L. Szewciw, G. McKinley, From ultra-soft slime to hard alpha-keratins: the many lives of intermediate filaments, Integrative and Comparative Biology 49 (1) (2009) 32–39.
[13] L.C.E. Struik, Free damped vibrations of linear viscoelastic materials, Rheologica Acta 6 (2) (1967) 119–129.
[14] R.H. Ewoldt, G.H. McKinley, Creep ringing in rheometry or how to deal with oft-discarded data in step stress tests, Rheology Bulletin 76(1) (2007).
[15] N.Y. Yao, R.J. Larsen, D.A. Weitz, Probing non-linear rheology with inertio-elastic oscillations, Journal of Rheology (4) (2008) 1013–1025.
[16] J.E. Herr, T.M. Winegard, M.J. O'Donnell, P.H. Yancey, D.S. Fudge, Stabilization and swelling of hagfish slime mucin vesicles, Journal of Experimental Biology 213 (7) (2010) 1092–1099.
[17] Z. Qin, L. Kreplak, M.J. Buehler, Hierarchical structure controls nanomechanical properties of vimentin intermediate filaments, PLoS ONE 4 (10) (2009) e7294.
[18] Z. Qin, M.J. Buehler, Molecular dynamics simulation of the alpha-helix to beta-sheet transition in coiled protein filaments: evidence for a critical filament length scale, Physical Review Letters 104 (19) (2010) 198304.
[19] T. Ackbarow, D. Sen, C. Thaulow, M.J. Buehler, Alpha-helical protein networks are self-protective and flaw-tolerant, PLoS ONE 4 (6) (2009) e6015.

[20] R.B. Bird, C.F. Curtiss, R.C. Armstrong, O. Hassager, Dynamics of Polymeric Liquids: Volume 2 Kinetic Theory, second ed., John Wiley and Sons, Inc, New York,, 1987.

[21] K.H. Ahn, K. Osaki, A network model for predicting the shear thickening behavior of a poly(vinyl alcohol) sodium-borate aqueous-solution, Journal of Non-Newtonian Fluid Mechanics 55 (3) (1994) 215–227.

[22] N. Phan-Thien, M. Safari-Ardi, A. Morales-Patio, Oscillatory and simple shear flows of a flour-water dough: a constitutive model, Rheologica Acta 36 (1) (1997) 38–48.

[23] J.A. Yosick, A.J. Giacomin, P. Moldenaers, A kinetic network model for nonlinear flow behavior of molten plastics in both shear and extension, Journal of Non-Newtonian Fluid Mechanics 70 (1–2) (1997) 103–123.

[24] N. Phan-Thien, M. Newberry, R.I. Tanner, Non-linear oscillatory flow of a soft solid-like viscoelastic material, Journal of Non-Newtonian Fluid Mechanics 92 (1) (2000) 67–80.

[25] A. Vaccaro, G. Marrucci, A model for the nonlinear rheology of associating polymers, Journal of Non-Newtonian Fluid Mechanics 92 (2–3) (2000) 261–273.

[26] H.G. Sim, K.H. Ahn, S.J. Lee, Large amplitude oscillatory shear behavior of complex fluids investigated by a network model: a guideline for classification, Journal of Non-Newtonian Fluid Mechanics 112 (2–3) (2003) 237–250.

[27] T.S.K. Ng, G.H. McKinley, R.H. Ewoldt, Power law gels in large amplitude oscillatory shear flow, Journal of Rheology, provisionally accepted.

[28] R.B. Bird, R.C. Armstrong, O. Hassager, Dynamics of Polymeric Liquids: Volume 1 Fluid Mechanics, second ed., John Wiley and Sons, Inc, New York,, 1987.

[29] R.B. Bird, Teaching with FENE dumbbells, Rheology Bulletin 76(1).

[30] R.H. Ewoldt, A.E. Hosoi, G.H. McKinley, New measures for characterizing nonlinear viscoelasticity in large amplitude oscillatory shear, Journal of Rheology 52 (6) (2008) 1427–1458.

[31] J.F. Marko, E.D. Siggia, Stretching DNA, Macromolecules 28 (1995) 8759–8770.

[32] C. Storm, J.J. Pastore, F.C. MacKintosh, T.C. Lubensky, P.A. Janmey, Nonlinear elasticity in biological gels, Nature 435 (7039) (2005) 191–194.

[33] L.L. Ma, J.Y. Xu, P.A. Coulombe, D. Wirtz, Keratin filament suspensions show unique micromechanical properties, Journal of Biological Chemistry 274 (27) (1999) 19145–19151.